Microchimica Acta (2020) 187:311
https://doi.org/10.1007/s00604-020-04263-1

ORIGINAL PAPER

Amplified electrochemical determination of UO_2^{2+} based on the cleavage of the DNAzyme and DNA-modified gold nanoparticle network structure

Chen Cao[1] · Jinquan Liu[2,3,4] · Shuangyang Tang[5] · Zhongran Dai[6] · Fubing Xiao[2,3] · Weiqing Rang[2] · Ling Liu[2] · Tuo Chen[2] · Yali Yuan[1] · Le Li[2,3,6]

Received: 31 October 2019 / Accepted: 3 April 2020

Abstract

A superior electrochemical biosensor was designed for the determination of UO_2^{2+} in aqueous solution by integration of DNAzyme and DNA-modified gold nanoparticle (DNA-AuNP) network structure. Key features of this method include UO_2^{2+} inducing the cleavage of the DNAzyme and signal amplification of DNA-AuNP network structure. In this electrochemical method, the DNA-AuNP network structure can be effectively modified on the surface of gold electrode and then employed as an ideal signal amplification unit to generate amplified electrochemical response by inserting a large amount of electrochemically active indicator methylene blue (MB). In the presence of UO_2^{2+}, the specific sites on DNA-AuNP network structure can be cleaved by UO_2^{2+}, releasing the DNA-AuNP network structure with detectable reduction of electrochemical response intensity. The electrochemical response intensity is related to the concentration of UO_2^{2+}. The logarithm of electrochemical response intensity and UO_2^{2+} concentration showed a wide linear range of 10~100 pM, and the detection limit reached 8.1 pM ($S/N = 3$). This method is successfully used for determination of UO_2^{2+} in water samples.

Keywords AuNPs · Electrochemical · Biosensor · UO_2^{2+} · Methylene blue · DNAzyme · Signal amplification · DNA-AuNP network · DPV · Water sample

Introduction

Uranium, a very important radioactive element, is widely distributed in the environment, such as the atmosphere, soil, or water [1]. In the past half century, uranium has been widely used in nuclear research, nuclear fuel, nuclear weapons, and other fields, so its demand has been gradually increased. Uranium mining, uranium enrichment, and spent fuel post-nuclear industrial processes are accompanied by the generation and release of a large amount of uranium-containing wastewater [2]. Uranium has both high chemotoxicity and radiotoxicity. Therefore, uranium contamination has posed a

Electronic supplementary material The online version of this article (https://doi.org/10.1007/s00604-020-04263-1) contains supplementary material, which is available to authorized users.

✉ Yali Yuan
yuanyali6439@126.com

✉ Le Li
usclile@126.com

[1] School of Chemistry and Chemical Engineering, University of South China, Hengyang 421001, Hunan, People's Republic of China

[2] School of Public Health, University of South China, Hengyang 421001, Hunan, People's Republic of China

[3] Key Laboratory of Health Hazard Factors Inspection and Quarantine, University of South China, Hengyang 421001, People's Republic of China

[4] State Key Laboratory of Chemo/Biosensing and Chemometrics, Hunan University, Changsha410082, PR China

[5] Institute of Pathogenic Biology, University of South China, Hengyang 421001, People's Republic of China

[6] Hunan Province Key Laboratory of Green Development Technology for Extremely Low Grade Uranium Resources, University of South China, Hengyang 421001, People's Republic of China

Published online: 04 May 2020

serious threat to the ecological system, which also will continue to hazard human health for a long time [3, 4]. Uranium is exposed in the water or soil sources can eventually enter the food chain and distribute throughout the human body via the bloodstream, which would cause some hereditary diseases, urinary system diseases, organ cancerization, and even death [5, 6]. Uranium exists in many forms in nature, among which UO_2^{2+} is the most common and stable chemical form [7]. The United State Environmental Protection Agency (US EPA) stipulates that the highest concentration of pollution levels for UO_2^{2+} in water is 130 nM [8]. Hence, it is essential to develop a novel determination method for UO_2^{2+}.

Various techniques have been developed to detect UO_2^{2+} in water, such as resonance light scattering(RLS) [9], surface-enhanced Raman spectroscopy(SERS) [10], and inductively coupled plasma mass spectrometry(ICP-MS) [11]. These methods have relative satisfied precision and accuracy, and researchers also have developed a lot of new methods for rapid, sensitive, and specific determination for UO_2^{2+}, including fluorescence [12, 13], colorimetry [14], and electrochemistry [15, 16]. Among these, the electrochemistry is more advantageous and has attracted much attention because it can meet the demand for detecting UO_2^{2+} rapidly on site owing to its simple operation and high sensitivity.

Nowadays, various electrochemical biosensors for UO_2^{2+} determination have been developed. In particular, DNAzyme-based electrochemical biosensor are especially attracting attention in UO_2^{2+} measurements because DNAzyme can be denatured and renatured without losing activity and display metal-binding affinity and specificity toward different metal ions. For instance, Tang et al. [17] constructed an electrochemical method for trace uranium based on UO_2^{2+} inducing the cleavage of the DNAzyme immobilized on the surface of gold electrode. Furthermore, to make ultrasensitive detection, the DNAzyme-based electrochemical biosensors combined with some amplification strategies were also developed. For example, Yun et al. [16] designed an ultrasensitive electrochemical detection method by integration of UO_2^{2+}-specific DNAzyme and hybridization chain reaction (HCR) amplification technology with the dynamic concentration range spanning from 0.05 to 4 nM and a detection limit of 20 pM. Our group [7] also proposed a novel electrochemical method for UO_2^{2+} by using UO_2^{2+}-dependent DNAzyme-induced mesoporous silica nanoparticles (MSNs) loaded with methylene blue (MB). This method showed a good linear correlation from 20 pM to 0.1 nM and the detection limit is 0.15 pM. Although the above DNAzyme-based electrochemical biosensor exhibited high sensitivity and specificity for UO_2^{2+} determination, it still is a meaningful challenge to design efficient and convenient electrochemical biosensors for UO_2^{2+} determination.

With the rapid development of nanotechnology, nanoparticles have been widely used as theon electrochemical sensors, such as TiO_2 nanoparticles [18], ZnO nanoparticles [19], $BiFeO_3$ nanoparticles [20], silica nanoparticles [7], and gold nanoparticles [21, 22]. Gold nanoparticles (AuNPs), as the widely used nanomaterials, possess some charming physical and chemical properties that make them excellent scaffolds for the fabrication of electrochemistry sensor. In particular, due to the attractive characteristics of biocompatibility and large specific surface area, AuNPs are capable to enrich some functional DNA and can provide the opportunity of being a platform for efficient modification of functional DNA loaded with some signal molecules for signal amplification. In addition, owning to the specificity of DNA base–pairing hybridization [23], the functional DNA modified [24] on the surface of AuNPs were hybridized with other functional DNA containing complementary sequence to initiate their assembly into DNA-modified gold nanoparticle (DNA-AuNP) network structure [25, 26]. As a result, the DNA-AuNP network structure was used as a signal amplification element for the activation of the electrochemical response of the incorporated electroactive substance and then enables the amplified electrochemical readout for the analysis of the targets. Of note, DNA-AuNP network structure is a promising approach because it does not require the participation of enzymes, and avoided the complicated procedures and slashing reaction conditions, resulting in an effective increase in sensitivity. In the past few years of research, the advent of DNA-AuNP network structure provided efficient approach for the amplified detection of metal ions [27], big molecules [28], proteins [29], and so on. To date, however, the use of DNA-AuNP network structure for UO_2^{2+} determination has been few reported yet. As such, it was demonstrated that the DNA-AuNP network structure–based electrochemical method can open a new horizon for the sensitivity determination of UO_2^{2+}.

Herein, a novel electrochemical method for high sensitive determination of UO_2^{2+} was constructed based on UO_2^{2+}-specific DNAzyme and DNA-AuNP network structure amplification. In this strategy, the DNA-AuNP network structure contained the UO_2^{2+}-specific DNAzyme which was consisted of enzyme chain (DNAS1) and substrate chain (DNAS2). As illustrated in Scheme 1, the gold electrode was firstly immobilized with DNAS1 via Au-S bond and then blocked with MCH. Subsequently, the DNAS1-modified electrode was incubated with some AuNPs-DNAS1 and AuNPs-DNAS2. In this work, a DNA-AuNP network structure would be formed on the surface of gold electrode. Thus, a large amount of methylene blue (MB) was inserted into the DNA-AuNP network structure, resulting in an amplified electrochemical signal [30]. Upon the introduction of UO_2^{2+}, the specific cleavage of DNAzyme would trigger the detachment of DNA-AuNP network structure from the gold electrode surface. As a result, a reduced electrochemical signal was detected with little MB that could be adsorbed on the surface of gold electrode. Therefore, the concentration of UO_2^{2+} can

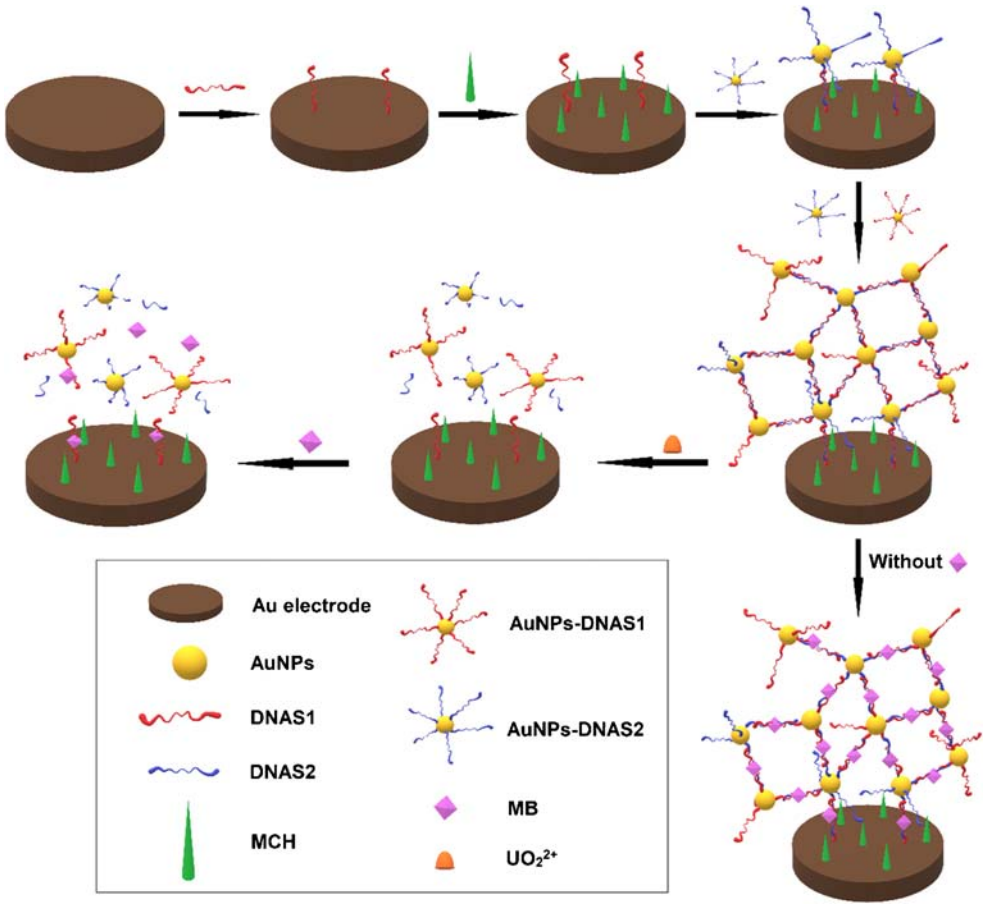

Scheme 1 Schematic representation of the electrochemical biosensor for UO_2^{2+} detection based on DNA-AuNPs network amplification signal

sensitively be detected through the electrochemical signals, which was attributed to the powerful amplification effect of the DNA-AuNP network structure. As a joint result of the UO_2^{2+}-specific DNAzyme and DNA-AuNP network structure amplification, the present electrochemical method opened up a new way and showed an attractive performance for the sensitive determination of UO_2^{2+}. The UO_2^{2+} determination in actual water samples was also indicated that the electrochemical method has the promise application in the treatment of water pollution and the protection of the environment.

Experimental

Material and instruments

Hydrogen tetrachloroaurate trihydrate ($HAuCl_4 \cdot 3H_2O$), methylene blue (MB), and sodium dodecyl sulfate (SDS) were obtained from Aladdin Biochemical Technology Co. Ltd. (Shanghai, China, http://www.aladdin-e.com/). Tris (2-carboxyethyl) phosphine hydrochloride (TCEP) and 6-mercapto-1-hexanol (MCH) were purchased from Meryer Chemical Technology Co.Ltd. (Shanghai, China, http://www.meryer.com/). Tris-base and ethylene diamine tetraacetic acid (EDTA) were purchased from Tianjin Damao Chemical Reagent Factory (Tianjin, China, http://www.dmreagent.com/). All other chemicals were of analytical reagent grade and without further purification prior to use. The solutions were configured by using ultrapure water (specific resistance of 18.2 MΩ cm) throughout the experiment. The DNA oligonucleotides used in this experiment were designed according to the previous report [31] and synthesized by Takara Biotechnology Co. Ltd. (Dalian, China, http://www.takara.com.cn/). The oligonucleotide sequence used in this study is listed in Table S1.

All electrochemical operations were performed on an electrochemical workstation (CHI660D Shanghai Chenhua Instrument Co., Ltd.). A conventional three-electrode system was used in all experimental operation, with the Au electrode (2 mm) as the working electrode, the KCl-saturated calomel electrode as the reference electrode, and the platinum electrode as auxiliary electrodes, and all measurements were made at room temperature (25 °C). In addition, the characteristics of the prepared AuNPs, AuNPs-DNA, and DNA-AuNP network structure was analyzed by UV-visible absorption spectrometer (UV-3900, Shimadzu Corporation, Japan), transmission electron microscope (JEM-2010, Hitachi, Japan), and scanning electron microscope (SEM, SU8010, Hitachi, Japan).

Preparation of AuNPs

The glass apparatus were soaked with fresh aqua regia (nitric acid:hydrochloric acid = 1:3) and rinse with plenty of ultrapure water. AuNPs with an average diameter of 16 nm were prepared according to standard sodium citrate reduction of $HAuCl_4$ [32]. Briefly, 50 mL of 0.01% $HAuCl_4$ solution was vigorously stirred and heated for 15 min until the solution began to reflux. Then 2 mL of 1% sodium citrate was quickly added to the boiling solution, and the reflux was continued for 15 min. After the color of the solution was changed from light yellow to purple, and then wine red, it indicated that the AuNPs were formed. The solution was stirred continually and cooled to room temperature. Finally, the prepared AuNP solution was filtered through a 22-μm filter and stored in a brown bottle at 4 °C.

Preparation of AuNPs-DNAS1 and AuNPs-DNAS2

The AuNPs were further modified with thiolated DNAS1 and DNAS2 according to previously reported methods. In brief, DNAS1 was treated with an excess of 5 mM TCEP for 1 h at 25 °C to activate the thiol group on DNAS1.Then, 150 μL of 5 mM TCEP-treated 10 μM DNAS1 solution was added to 500-μL AuNPs and incubated at 4 °C for 12 h. Subsequently, 10 μL of 1% SDS was added and shaken for 1 h to stabilize the AuNPs. Then the AuNPs-DNAS1 were aged for 12 h by adding 50 μL of 0.5 M NaCl solution. The AuNPs-DNAS1 solution was centrifuged at 8000 rpm for 10 min, and the supernatant was aspirated to remove excess reagent. It was washed with 0.01 M phosphate-buffered solution (pH 7.4) and centrifuged 3 times. The obtained AuNPs-DNAS1 was obtained and stored in TE buffer (pH 8.0) for further use. The AuNPs-DNAS2 solution was prepared in the same manner as AuNPs-DNAS1.

Biosensor interface preparation

Firstly, the Au electrode (2 mm in diameter) was polished to the mirror surface with alumina powder of 1.0, 0.3, and 0.05 μm sequentially, followed by sonication for 5 min in ultrapure water, ethanol, and ultrapure water, respectively. Then the electrode was soaked in fresh piranha solution (98% H_2SO_4 and 30% H_2O_2 by volume ratio of 3:1) for 10 min to remove the organic solvent and cleaned with ultrapure water completely, followed by rinsing with a large amount of ultrapure water and drying under nitrogen. Secondly, 10 μL of 0.2 μM TCEP-activated DNAS1 solution was dropped on the electrode surface and placed at 4 °C for 12 h, with the lid covered to prevent liquid evaporation. To block the unbound site on gold electrode, the electrode was immersed into 1 mM MCH solution at room temperature for 1 h. The DNAS1-modified electrode was then incubated with the solution with 10-μL AuNPs-DNAS2 for 2 h at 25 °C. During this process, hybridization of DNAS1 with AuNPs-DNAS2 may result in the assembly of AuNP-DNAS2 on the electrode to form the inner layer. After that, 10 μL of the AuNPs-DNAS1 solution was further drooped for 4 h. As a result, AuNPs-DNAS1 can continue hybridization with AuNPs-DNAS2 to form an external layer. Therefore, DNA-AuNP network structure was constructed by repeatedly alternate interaction. Prior to the test, the electrodes were immersed in 10 mL of 20 μM MB (20 μM MB and 20 mM KCl in phosphate-buffered solution (pH 7.4) for 10 min, and then washed with ultrapure water.

Electrochemical detection

Biosensor modification process was measured by cyclic voltammetry (CV) and electrochemical impedance spectroscopy (EIS). The concentration of analyte was detected by differential pulse voltammetry (DPV). Both CV and EIS scans were performed in 5 mM $[Fe(CN)_6]^{3-/4-}$ containing 0.1 M KCl. The parameters of CV are as follows: scan rate, 0.1 V/s; high potential, 0.8 V; low potential, − 0.3 V; sample interval, 0.001 V; quiet time, 2 S; sensitivity, 1×10^{-5} A/V. The parameters of EIS are as follows: frequency range, 0.1 Hz~100 kHz; amplitude, 0.005 V; quiet time, 2 S. DPV measurements were performed in a phosphate-buffered solution containing 40 mM NaCl with the following parameters: initial potential, − 0.50 V; final potential, 0 V; increment potential, 0.004 V; amplitude,0.05 V; pulse width,0.05 S; sampling width, 0.0167 S; pulse period, 0.2 S; quiet time, 2 S.

Results and discussion

Characterization of AuNPs, AuNPs-DNA, and DNA-AuNP network

The UV-visible absorption spectroscopy (UV-vis) was used to characterize the AuNPs and AuNPs-DNA. As shown in Fig. S1a, pure AuNPs have a characteristic absorption peak at a wavelength of 519 nm (curve 1). In contrast, the AuNPs modified with DNAS1 and DNAS2 resulted in a slight shift in the peak from 519 to 522 nm (curve 2 and curve 3), which was consistent with previous reports [33]. This result indicated that DNAS1 and DNAS were successfully modified on the surface of AuNPs. In addition, the TEM and SEM were also used to characterize the morphology and structure of AuNPs, AuNPs-DNA, and DNA-AuNP network. Figure 1a shows that pure AuNPs exhibited monodispersed spherical particles with an average size of about 16 nm. Fig. S1b shows the TEM of AuNPs-DNA complex, the image was almost identical to AuNPs, which probably due to the DNA strand was too small and can be ignored compared with gold nanoparticles. The DNA-AuNP network structure is shown in Fig. 1b, a large number of the AuNPs-DNAS1 and AuNPs-DNAS2 aggregated together, and thousands of nanoparticles were connected by DNAzyme to form a network structure. Fig. S1c shows the SEM image of

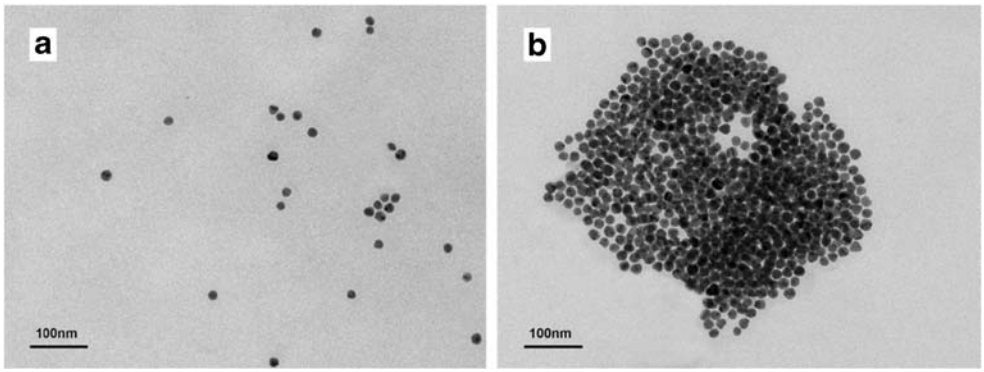

Fig. 1 TEM of **a** AuNPs and **b** DNA-AuNP network structure

pure AuNPs. Fig. S1d is the SEM image of DNA-AuNP network structure, and it can be seen that a white polymer was shown in the figure, which may be the result of a large number of DNAzymes linking the dispersed AuNPs together. DNAzyme was a poorly conductive material, which causes a high-energy electron beam generated by a higher accelerating voltage to generate a charging effect during scanning of a sample, which was consistent with the results of TEM, demonstrating that the hybridization reaction on the electrode surface was processed successfully as expected.

Electrochemical characterization of electrode modification process

To confirm the modification process on the electrode surface, the CV for each step of Au electrode preparation was performed. As Fig. 2a shows, the bare Au electrode revealed a pair of comparatively symmetrical redox peaks, the peak potential difference was less than 100 mV (curve 1). After self-assembly of DNAS1 on the electrode surface, the current response reduced slightly and the separation degree of two peaks was increased (curve 2), which was caused by the electrostatic repulsion between the negatively charged DNAS1 and $[Fe(CN)_6]^{3-/4-}$. It was indicated that DNAS1 was successfully modified on the Au electrode. To avoid the non-specific adsorption of other substances and hold the DNAS1 chain to stand upright, MCH was assembled onto the DNAS1-modified Au electrode. However, the peak current decreased greatly and the separation degree of two peaks increased significantly compared with those of before (curve 3), which may be due to the sealing effect of MCH to penetration of redox species to the electrode surface. By the continued addition of just AuNPs-DNAS2, the peak current decreased to some extent and the separation degree of two peaks was expanded obviously (curve 4). After the hybridization between two types of AuNP-DNA, the lowest redox peak (curve 5) was obtained due to the suppression of electron transfer when the formed DNA-AuNP network structure was attached onto the surface. All of these CV curves indicated that the Au electrode modification was processed successfully.

EIS was also an important means to measure the features of modified gold electrode. The diameter of semicircle was equivalent to the value of charge transfer resistances (R_{ct}) and the increase of diameter indicated the heightening in the interface impedance. As shown in Fig. 2b, the impedance of the bare Au electrode is quite small (curve 1), and the R_{ct} increased gradually with the modification of DNAS1 (curve 2), MCH (curve 3), AuNPs-DNAS2 (curve 4), and DNA-AuNP network structure (curve 5) to the Au electrode surface in sequence. The equivalent electrical circuit was used to fit the EIS data and the calculated R_{ct} values are shown in Table S2. It can be seen that the Au electrode showed a tiny R_{ct} value (179.8 Ω). When DNAS1 was self-assembled onto the Au electrode, the R_{ct} value (2126 Ω) was slightly increased, which may be ascribed to DNAS1 blocking the electron transfer on the surface of the gold electrode. The R_{ct} value

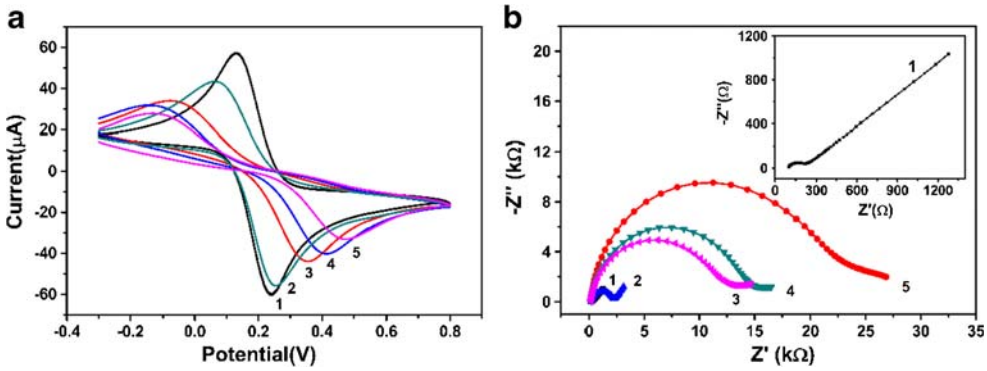

Fig. 2 **a** Cyclic voltammetry and **b** Nyquist diagrams of the biosensor at different stages: bare Au (curve 1), Au/DNAS1 (curve 2), Au/DNAS1/MCH (curve 3), Au/DNAS1/MCH/AuNPs-DNAS2 (curve 4), Au/DNAS1/MCH/ DNA-AuNPs network (curve 5). The potential range of CV is from − 0.3 to 0.8 V at 0.1 V/s and the frequency range of EIS is 0.1 Hz to 10 kHz with 5 mV as the amplitude

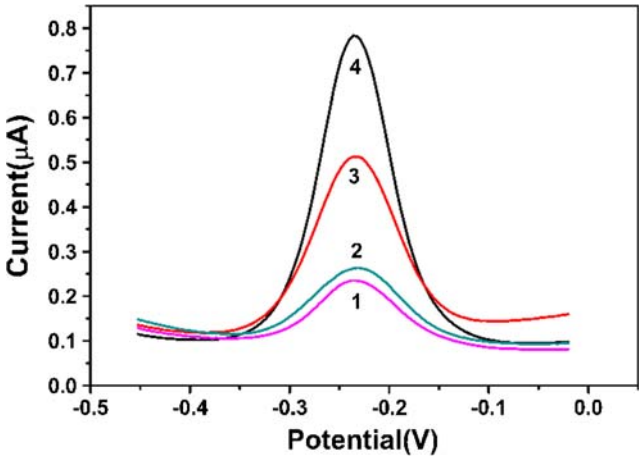

Fig. 3 Differential pulse voltammograms of the DNAS1 modified gold electrode (curve 1), in the presence of AuNPs-DNAS1 without AuNPs-DNAS2 (curve 2), in the presence of AuNPs-DNAS2 without AuNPs-DNAS1 (curve 3), in the presence of AuNPs-DNAS1 and AuNPs-DNAS2 (curve 4)

(12,163 Ω) increased obviously after MCH was added on the electrode surface, which was attributed to the fact that the MCH can obstruct the electron transfer. However, with participation of AuNPs-DNAS2, the R_{ct} value rose (14,226 Ω). When the AuNPs-DNAS1 and AuNPs-DNAS2 hybridized to form a DNA-AuNP network structure, R_{ct} value (22,514 Ω) increased dramatically, indicating that the DNA-AuNP network structure was successfully modified on the electrode surface. The results in EIS were consistent with those in the CV method, which further illustrated that the biosensor had been fabricated successfully.

Feasibility analysis of biosensors

DPV, as a very sensitive determination method, can be used to evaluate the feasibility of this method for UO_2^{2+} determination. As shown in Fig. 3, the gold electrode modified with DNAS1 showed a very small DPV peak (curve 1). The peak current increased to some extent after the AuNPs-DNAS2 modifying process (curve 3), indicating that AuNPs-DNAS2 was connected to the electrode surface and loaded with some MB. In comparison, the peak current as a slight increase after the AuNPs-DNAS1 was introduced (curve 2), which were attributed to the nonspecific adsorption. Clearly, with integrating the AuNPs-DNAS1 and AuNPs-DNAS2 together, a peak current raise by leaps and bounds was obtained (curve 4). It was indicated that the sensing interface has been fabricated successfully. These results indicated that the electrical signals can be amplified by DNA-AuNP network structure more effectively.

Optimization of method

The following parameters were optimized: (a) assay pH value, (b) reaction temperature, and (c) incubation time. Respective text and figures on optimizations are given in the Electronic Supporting Material (Fig. S2). In short, the following experimental conditions were found to give best results: (a) the best assay pH value used in the experiment was 6.0; (b) reaction temperature was 35 °C; (c) incubation time was 6 h.

UO_2^{2+} detection

Since the current signal was straightly related to the amount of UO_2^{2+}, under the optimum conditions, the performance of biosensor was studied by varying UO_2^{2+} concentration. As shown in Fig. 4a, with UO_2^{2+} concentration changed from 0 to 1000 pM, the current signal decreased progressively. Figure 4b is a calibration plot for different concentrations of UO_2^{2+} ions. As shown in the inset of Fig. 3b, when the UO_2^{2+} concentration was in the range of 10~100 pM, the logarithm of the concentration had a good linear relationship with the current, with the correlation coefficient $R^2 = 0.9923$. The

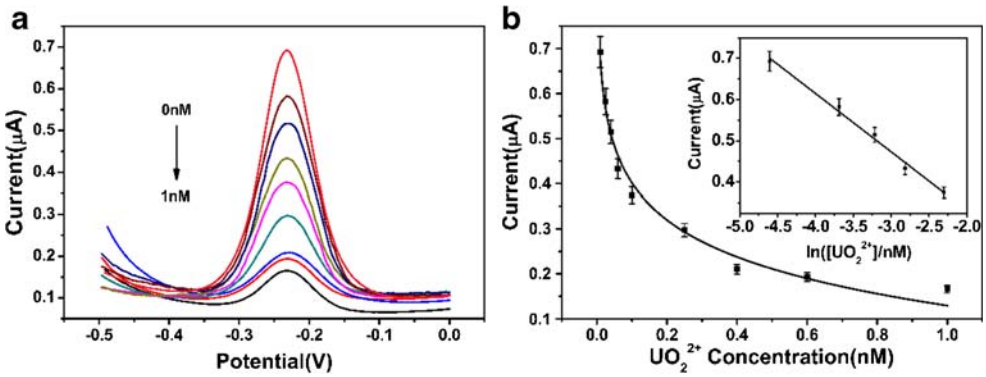

Fig. 4 **a** The DPV curve of the sensor in the presence of different concentrations of UO_2^{2+} ions, from top to bottom (0, 0.01, 0.025, 0.04, 0.06, 0.1, 0.25, 0.4, 0.6, 1 nM). The solution was tested in 10 mM phosphate-buffered solution. **b** Calibration plot of biosensors for different concentrations of UO_2^{2+} ions. The inset showed a linear relationship between peak current phase and UO_2^{2+} concentration over a concentration range of 10 to 100 M. DPV was recorded in phosphate buffered solution containing 40 mM NaCl from − 0.5 to 0 V under a pulse amplitude of 50 mV

linear equation is $I(\mu A) = -0.1415\ln[C] + 0.0487$, where I is the peak current and C is the concentration of UO_2^{2+}. The detection limit was 8.1 pM (based on S/N = 3). As compared with other methods of UO_2^{2+} determination in Table 1, the detection of limit (LOD) by this method has at least one order lower of magnitude than that by other methods, which are mainly ascribed to two reasons: firstly, the strong binding affinity between DNAzyme and UO_2^{2+} can provide relatively high determination sensitivity; secondly, DNA-AuNP network structure was utilized to adsorb more MB on the electrode surface. In consequence, the determination signal was effectively amplified. It can be seen that the biosensors were used to detect UO_2^{2+} in aqueous solution simply, sensitively, and effectively.

Electrochemical biosensor selectivity, stability and reproducibility

To explore the selectivity of this biosensor, a series of common metal ions were used and tested, including Mg^{2+}, Ca^{2+}, Zn^{2+}, Fe^{3+}, Cu^{2+}, Co^{2+}, K^+, Ni^{2+}, VO_2^+, Cd^{2+}, and Mn^{2+}(each 10 nM) under the optimum situations. Figure 5 depicted the DPV responses of the biosensors to different metal ions. The biosensor performance was denoted by the relative intensity $\Delta I = (I - I_0)$, where I_0 and I are the peak currents of the biosensor in the lack and exist of metal ions. Although the concentration of the interfering substance reached 10 times than that of the analyte, the peak current change ΔI of all the higher interfering ions was much smaller than that of the low concentration UO_2^{2+}. This result indicated that the response of the method to UO_2^{2+} was unaffected by the other metal ions. Therefore, this method had good selectivity for UO_2^{2+}. The good performance in selectivity was mainly attributed to the specific cleavage of UO_2^{2+} for DNAzymes.

In addition, the stability was an important indicator for biosensor performance, so the storage stability of this biosensor was also studied. When the fabricated electrode was stored in ultrapure water at 4 °C for 10 days, 91.56% of the initial current was still reserved. This consequence proved that the prepared biosensor had nice storage stability.

Table 1 Performance of different UO_2^{2+} sensors

Method	Linear range	Detection limit	References
Fluorescence	0~0.6 μM	0.039 μM	[13]
Fluorescence	0~25 nM	0.19 nM	[23]
SERS	0.2~5 mM	200 nM	[10]
RLS	13.6~150 nM	4.09 nM	[34]
Colorimetric	12–160 μM	1.86 μM	[35]
Electrochemical	10~100 pM	8.1 pM	This work

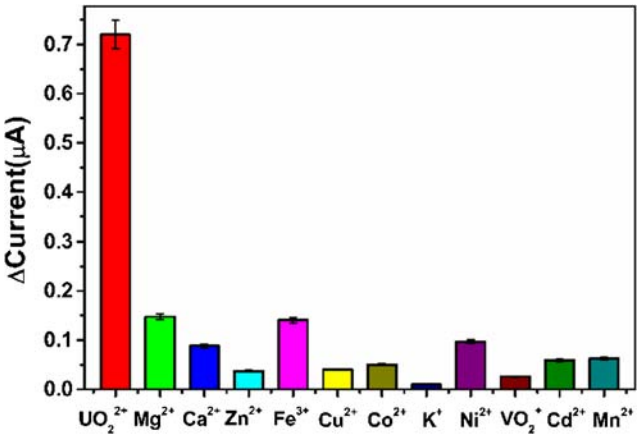

Fig. 5 Selectivity of the electrochemical biosensor towards the target UO_2^{2+} against that towards Mg^{2+}, Ca^{2+}, Zn^{2+}, Fe^{3+}, Cu^{2+}, Co^{2+}, K^+, Ni^{2+}, VO_2^+, Cd^{2+}, and Mn^{2+}

To examine the reproducibility of the method, five different modified electrodes were prepared and incubated with uranyl ions of the same solubility, and the electrochemical signals were measured. The relative standard deviation (RSD) of the results using the five electrodes was 7.20%. Then, the experiment was performed five times with the same electrode. The RSD of the obtained electrochemical signal was 2.15%. The experimental results show that the method has excellent repeatability for the determination of UO_2^{2+}.

Application of biosensors for water samples

To assess the practical suitability of the raised method in actual water samples, the method was used to determine trace UO_2^{2+} in tap water and water from Xiangjiang River by addition of standard uranium solutions. Actual water samples were filtered with a 0.45-μm filter. For a spiked sample, a known amount of UO_2^{2+} was added into the river and tap water samples. Two spiked samples with the UO_2^{2+} concentration of 0.025 nM and 0.05 nM were analysed. The results are listed in Table S3. The recovery ranged from 96 to 101.5% and the RSD was in the range 3.47 to 7.93%. These results demonstrated that the method holds large potential for the quantification of UO_2^{2+} in complex water samples.

Conclusion

This work presented a sensitive and selective electrochemical nanoprobe for the determination of UO_2^{2+}. Taking the signal amplification of DNA-AuNP network combined with MB and the specific cleavage of DNAzyme, a relatively lower detection limit of 8 pM was achieved, which was lower than some conventional methods for UO_2^{2+}. Compared with some conventional methods, our methods offered some fascinating advantage, such as ease of operation, time saving in

determination, and good sensitivity and specificity for UO_2^{2+} determination. Given the important roles of UO_2^{2+} determination in the complex water samples, it demonstrated that the biosensor has potential for analytical application in real samples. For this method, it has excellent selectivity for metal cations, while other chemicals (such as humic acid, fulvic acid, tannic acid, or other organic species with potential redox activity) in water samples have not been thoroughly explored. In addition, the proposed method would provide versatility for other pollutant (such as drugs, pesticides, fungicides, catechol, biogenic amines, and other heavy metal ions) detection by replacing the corresponding DNA sequence. It is indicated that the method shows great value for the treatment of water pollution and the protection of the environment.

Funding information This research was supported by the Key R&D Program of Hunan Province (2018SK2029), the National Natural Science Foundation of China (11405081, 21906077), the Natural Science Foundation of Hunan Province (2018JJ3452), the Open Project Program of the State Key Laboratory of Chemo/Biosensing and Chemometrics, Hunan University (2018010), the science and technology project of Hengyang (2018KJ123), and the Fund of Hengyang Key Laboratory (2018KJ110).

Compliance with ethical standards

Conflict of interest The author(s) declare that they have no competing interests.

References

1. Astrid B, Christoph H, Atsushi I-O (2018) Interaction of uranium(VI) with α-amylase and its implication for the enzyme activity. Chem Res Toxicol 31:1032–1041. https://doi.org/10.1021/acs.chemrestox.8b00106
2. Lu W, Li L, Ding DX, Dai ZR, Tang SY, Cao C, Liu L, Chen T (2018) Selective adsorption of uranium (VI) by calix[6]arene-modified magnetic graphene oxide. J Nanosci Nanotechnol 18:8160–8168. https://doi.org/10.1166/jnn.2018.16408
3. Rossberg A, Abe T, Okuwaki K, Barkleit A, Fukuzawa K, Nakano T, Mochizuki Y, Tsushima S (2019) Destabilization of DNA through interstrand crosslinking by UO_2^{2+}. Chem Commun 55:2015–2018. https://doi.org/10.1039/c8cc09329f
4. Hua MX, Yang S, Ma JQ, He WW, Kuang LJ, Hua DB (2018) Highly selective and sensitive determination of uranyl ion by the probe of CdTe quantum dot with a specific size. Talanta 190:278–283. https://doi.org/10.1016/j.talanta.2018.08.012
5. Ma FQ, Dong BR, Gui YY, Cao M, Han L, Jiao CS, Lv HT, Hou JJ, Xue Y (2018) Adsorption of low-concentration uranyl ion by amidoxime polyacrylonitrile fibers. Ind Eng Chem Res 57:17384–17393. https://doi.org/10.1021/acs.iecr.8b03509
6. Roozbahani GM, Chen XH, Zhang YW, Xie RQ, Ma R, Li DE, Li HZ, Guan XY (2017) Peptide-mediated nanopore detection of uranyl ions in aqueous media. ACS Sensors 2:703–709. https://doi.org/10.1021/acssensors.7b00210
7. Wen Y, Yuan YL, Li L, Ma DD, Liao Q, Hou SY (2017) Ultrasensitive DNAzyme based amperometric determination of uranyl ion using mesoporous silica nanoparticles loaded with methylene blue. Microchim Acta 184:3909–3917. https://doi.org/10.1007/s00604-017-2397-7
8. Ansoborlo E, Lebaron-Jacobs L, Prat O (2015) Uranium in drinking-water: a unique case of guideline value increases and discrepancies between chemical and radiochemical guidelines. Environ Int 77:1–4. https://doi.org/10.1016/j.envint.2014.12.011
9. Xu L, Xiao XL, Wang J, Peng PC, Jiang M, Liao LF (2017) The detection of uranium(VI) with a synthesized ditopic bidentate ligand as probe by resonance light scattering. J Radioanal Nucl Chem 312:59–66. https://doi.org/10.1007/s10967-017-5199-9
10. Jiang JL, Wang SF, Deng H, Wu HX, Chen J, Liao JS (2018) Rapid and sensitive detection of uranyl ion with citrate-stabilized silver nanoparticles by the surface-enhanced Raman scattering technique. R Soc Open Sci 5:181099. https://doi.org/10.1098/rsos.181099
11. Möser C, Kautenburger R, Philipp Beck H (2012) Complexation of europium and uranium by humic acids analyzed by capillary electrophoresis-inductively coupled plasma mass spectrometry. Electrophoresis 33:1482–1487. https://doi.org/10.1002/elps.201100652
12. Yun W, Wu H, Yang ZH, Wang RQ, Wang CJ, Yang LZ, Tang YJ (2019) A dynamic, ultra-sensitive and "turn-on" strategy for fluorescent detection of uranyl based on DNAzyme and entropy-driven amplification initiated circular cleavage amplification. Anal Chim Acta 1068:104–110. https://doi.org/10.1016/j.aca.2019.04.018
13. Lin N, Ren WS, Hu JN, Gao B, Yuan DP, Wang XL, Fu J (2019) A novel tetraphenylethene-based fluorescent sensor for uranyl ion detection with aggregation-induced emission character. Dyes Pigments 166:182–188. https://doi.org/10.1016/j.dyepig.2019.02.048
14. Saha A, Neogy S, Rao DRM, Deb SB, Saxena MK, Tomar BS (2019) Colorimetric and visual determination of ultratrace uranium concentrations based on the aggregation of amidoxime functionalized gold nanoparticles. Microchim Acta 186:183–192. https://doi.org/10.1007/s00604-019-3292-1
15. Yun W, Cai DZ, Jiang JL, Wang XF, Liao JS, Zhang PC, Sang G (2016) An ultrasensitive electrochemical biosensor for uranyl detection based on DNAzyme and target-catalyzed hairpin assembly. J Microchim Acta 183:1425–1432. https://doi.org/10.1007/s00604-016-1778-7
16. Yun W, Jiang JL, Cai DZ, Wang XF, Sang G, Liao JS, Lu TC, Yan KP (2016) Ultrasensitive electrochemical detection of UO_2^{2+} based on DNAzyme and isothermal enzyme-free amplification. RSC Adv 6:3960–3966. https://doi.org/10.1039/c5ra22773a
17. Tang Q, Yuan YL, Xiao XL, Guo P, Hu JB, Ma DD, Gao YY (2013) DNAzyme based electrochemical sensors for trace uranium. Microchim Acta 180:1059–1064. https://doi.org/10.1007/s00604-013-1021-8
18. Shetti NP, Nayak DS, Malode SJ, Kakarla RR, Shukla SS, Aminabhavi TM (2018) Sensors based on ruthenium-doped TiO2 nanoparticles loaded into multi-walled carbon nanotubes for the detection of flufenamic acid and mefenamic acid. Anal Chim Acta 1051:58–72. https://doi.org/10.1016/j.aca.2018.11.041
19. Shettia NP, Bukkitgara SD, Reddyb KR, Reddyc CV, Aminabhavid TM (2019) ZnO-based nanostructured electrodes for electrochemical sensors and biosensors in biomedical applications. Biosens Bioelectron 141:111417. https://doi.org/10.1016/j.bios.2019.111417
20. Basavarajappa PS, Seethya BNH, NagarajuGanganagappa EKB, Kakarla RR (2018) Enhanced Photocatalytic activity and biosensing of gadolinium substituted BiFeO3 nanoparticles. ChemistrySelect 3:9025–9033. https://doi.org/10.1002/slct.201801198
21. Chen DL, Zhang M, Ma MY, Hai H, Li JP, Shan Y (2019) A novel electrochemical DNA biosensor for transgenic soybean detection based on triple signal amplification. Anal Chim Acta 1078:24–31. https://doi.org/10.1016/j.aca.2019.05.074

22. Chen X, Huang J, Zhang S, Mo F, Su SS, Li Y, Fang LC, Deng J, Huang H, Luo ZX, Zheng JS (2019) Electrochemical biosensor for DNA methylation detection through hybridization chain-amplified reaction coupled with a tetrahedral DNA nanostructure. ACS Appl Mater Interfaces 11:3745–3752. https://doi.org/10.1021/acsami.8b20144
23. Feng ML, Gu CM, Sun YP, Zhang SY, Tong AJ, Xiang Y (2019) Enhancing catalytic activity of uranyl-dependent DNAzyme by flexible linker insertion for more sensitive detection of uranyl ion. Anal Chem 91:6608–6615. https://doi.org/10.1021/acs.analchem.9b00490
24. Chen SQ, Frank Cheng Y, Voordouw G (2018) Three-dimensional graphene nanosheet doped with gold nanoparticles as electrochemical DNA biosensor for bacterial detection. Sensors Actuators B Chem 262:860–868. https://doi.org/10.1016/j.snb.2018.02.093
25. Wang ZH, Sun N, He Y, Liu Y, Li JH (2014) DNA assembled gold nanoparticles polymeric network blocks modular highly sensitive electrochemical biosensors for protein kinase activity analysis and inhibition. Anal Chem 86:6153–6159. https://doi.org/10.1021/ac501375s
26. Xie H, Zhang QQ, Wang Q, Chai YQ, Yuan YL, Yuan R (2015) Fe_3O_4NPs mediated nonenzymatic electrochemical immunosensor for the total protein of Nosema bombycis detection without addition of substrate. Chem Commun 51:7132–7135. https://doi.org/10.1039/c5cc01658d
27. Tang XM, Liu HX, Zou BH, Tian DB, Huang H (2012) A fishnet electrochemical Hg^{2+} sensing strategy based on gold nanoparticle-bioconjugate and thymine-Hg(2+)-thymine coordination chemistry. Analyst 137:309–311. https://doi.org/10.1039/c1an15908a
28. Gao Y, Deng XL, Wen W, Zhang XH, Wang SF (2017) Ultrasensitive paper based nucleic acid detection realized by three-dimensional DNA-AuNPs network amplification. Biosens Bioelectron 92:529–535. https://doi.org/10.1016/j.bios.2016.10.068
29. Zhang J, Yuan YL, biXie S, Chai YQ, Yuan R (2014) Amplified amperometric aptasensor for selective detection of protein using catalase-functional DNA-PtNPs dendrimer as a synergetic signal amplification label. Biosens Bioelectron 60:224–230. https://doi.org/10.1016/j.bios.2014.04.024
30. Cheng H, Liu JQ, Ma WJ, Duan SD, Huang J, He XX, Wang KM (2018) Low background cascade signal amplification electrochemical sensing platform for tumor-related mRNA quantification by target-activated hybridization chain reaction and electroactive cargo release. Anal Chem 90:12544–12552. https://doi.org/10.1021/acs.analchem.8b02470
31. Zhang HY, Ruan YJ, Lin L, Lin MG, Zeng XX, Xi ZM, Fu FF (2015) A turn-off fluorescent biosensor for the rapid and sensitive detection of uranyl ion based on molybdenum disulfide nanosheets and specific DNAzyme. Spectrochim Acta A Mol Biomol Spectrosc 146:1–6. https://doi.org/10.1016/j.saa.2015.02.113
32. Liu JW, Lu Y (2006) Preparation of aptamer-linked gold nanoparticle purple aggregates for colorimetric sensing of analytes. Nat Protoc 1:246–252. https://doi.org/10.1038/nprot.2006.38
33. Jing XY, Cao XQ, Wang L, Lan T, Li YY, Xie GM (2014) DNA-AuNPs based signal amplification for highly sensitive detection of DNA methylation, methyltransferase activity and inhibitor screening. Biosens Bioelectron 58:40–47. https://doi.org/10.1016/j.bios.2014.02.035
34. Zhou B, Shi L-F, Wang Y-S, Yang H-X, Xue J-H, Liu L, Wang Y-S, Yin J-C, Wang J-C (2013) Resonance light scattering determination of uranyl based on labeled DNAzyme–gold nanoparticle system. Spectrochim Acta A Mol Biomol Spectrosc 110:419–424. https://doi.org/10.1016/j.saa.2013.03.036
35. Zhang DY, Chen Z, Omar H, Deng L, Khashab NM (2015) Colorimetric peroxidase mimetic assay for uranyl detection in sea water. ACS Appl Mater Interfaces 7:4589–4594. https://doi.org/10.1021/am507361x